



# OPEN Topoclimatic factors create favourable conditions for carbon-dense forests in the Central Himalayas

Shiva Khanal<sup>1✉</sup>, Rachael H. Nolan<sup>2</sup>, Belinda E. Medlyn<sup>2</sup> & Matthias M. Boer<sup>2</sup>

The Central Himalayas, characterized by one of the most pronounced elevation gradients globally, harbor forest stands of high carbon density. With estimated forest aboveground biomass (AGB) densities of up to 1000 t ha<sup>-1</sup>, these forests are among the most carbon-rich ecosystems within the Himalayas and high mountain ranges globally. However, existing global and regional models of forest carbon distribution fail to accurately capture the remarkable carbon density observed in these Himalayan forest stands. Our objective was to quantify how fine-scale topoclimatic conditions influence the spatial variability of AGB, with the aim of identifying the environmental factors that contribute to the high carbon density observed in high mountain forests of Nepal. Our analysis focused on quantifying the contribution of terrain-driven variation in climatic energy and water availability in creating favourable site conditions for carbon-dense forests. We found that extreme forest carbon density is associated with distinct topographic settings related to slope, aspect and curvature that provide a combination of adequate levels of both climatic energy and water availability, while forest carbon was reduced in topographic positions associated with high likelihood of disturbance such as avalanches and mass movements. Our findings shed light on the intricate relationship between topoclimatic factors and conditions for carbon storage in high-elevation forests, providing valuable insights for conservation and management strategies in mountainous regions.

**Keywords** Forest carbon, High elevation, Central Himalayas, Topoclimate, Climatic energy, Climatic water availability

Models of global or continental-scale forest biomass distributions often misrepresent small-scale variations in forest structure, particularly in environmentally heterogeneous regions of the world's major mountain ranges<sup>1,2</sup>. In this study we focus on the Central Himalayas, which extend from subtropical to alpine ecoregions and harbour forest stands exceeding 1000 t ha<sup>-1</sup> aboveground biomass (AGB), ranking among the most carbon-dense forest globally<sup>3,4</sup>. However, the factors sustaining this high carbon density in high-elevation forests remain poorly understood. Previous studies on Himalayan forest structure and composition have been predominantly local<sup>5</sup>, while dendrochronological approaches have investigated climate-growth relationships in small areas only (e.g.,<sup>6–8</sup>). The pronounced relief and associated heterogeneity of topoclimatic heterogeneity in mountainous regions<sup>9</sup> make it challenging to generalize these findings.

Forest biomass is constrained by resource availability, including a stable substrate, climatic energy, and moisture<sup>10</sup>. In the mountainous regions, broad-scale variation in forest carbon density is therefore expected to be a function of long-term climate patterns, relief features, and lithology. However, at smaller scales, topography modulates the availability of water and light within specific elevation zones<sup>11</sup>, shaping forest habitat conditions. Topographic position influences local climatic factors like snow deposition<sup>12</sup>, wind exposure<sup>13</sup>, rainfall<sup>14</sup>, solar radiation and air temperature<sup>15</sup>, impacting the length of the growing season<sup>16</sup>, composition, structure, and productivity of forests<sup>17,18</sup>.

The forest AGB is primarily determined by long-term net primary productivity (NPP), representing the energy produced after accounting for respiration, maintenance, and mortality<sup>19</sup>. Numerous studies have shown strong NPP-AGB relationships across diverse environments (e.g.,<sup>20–24</sup>), including high elevation mountainous regions<sup>25–27</sup>. Here, we posit that by modelling the spatial variability of climatic factors influencing plant growth, such as the availability of climatic energy and water, broad-scale NPP variation can be approximated. Higher

<sup>1</sup>Forest Research and Training Center, Kathmandu, Nepal. <sup>2</sup>Hawkesbury Institute for the Environment, Western Sydney University, Sydney, Australia. ✉email: khanalshiva1@gmail.com

NPP is expected where climatic energy and water are abundant, while lower NPP is expected where either climatic energy or water is limiting<sup>28–30</sup>.

Topographic position and terrain characteristics also impose constraints on forest biomass by influencing the disturbance regimes<sup>31</sup>. Elevation, relief, and terrain features introduce variations in the nature and intensity of human-induced disturbances, such as land use activities (e.g., grazing and forest product collection) and infrastructure development (e.g., roads). Additionally, natural disturbances like avalanches, mudflows, landslides, and gully erosion are associated with specific topographic positions as well<sup>32,33</sup>, often leading to locally reduced forest productivity compared to the climatic potential for the broader landscape or region<sup>34</sup>.

The extremely heterogeneous relief and relatively sparse coverage by meteorological station in the Central Himalayas lead to uncertainties in gridded climatic datasets, constraining their ability to capture the heterogeneity in precipitation<sup>35</sup>, radiation<sup>36</sup>, and air temperature<sup>37</sup> induced by topographic diversity. Terrain attributes such as slope gradient/aspect, profile/plan curvature and specific drainage area have been shown to capture landscape-scale variation in air temperature, radiation budgets<sup>38</sup>, moisture conditions<sup>39</sup>, and soil properties such as depth, texture, rock fragments, drainage, and soil moisture regimes<sup>40</sup> related to topographic position.

This study addresses a critical knowledge gap in understanding how fine-scale topoclimatic variation constrains spatial patterns of forest biomass distribution in mountainous landscapes. While global models often overlook the spatial complexity of forest carbon stocks in rugged terrain, we focus on the Central Himalayas to assess how terrain-driven variation in moisture availability, energy input, and disturbance exposure shapes the distribution of high-biomass forest stands. This study builds on earlier work that utilized plot-level data from Nepal's national forest inventory<sup>41</sup> to investigate broad environmental drivers of forest biomass distribution<sup>31</sup>. Previous research confirmed elevational gradients in forest carbon stocks and identified the roles of tree species composition, structure, and topography in mediating relationships between forest carbon pools and environmental variables<sup>4</sup>. Extending this foundation, the current study examines more specifically how climatic water and energy availability influences the distribution of high biomass forest stands in Nepal's high-elevation forests. This study aims to model the contribution of topoclimatic factors to variation of forest AGB in high mountain ecosystems of the Central Himalayas, and thereby improve our understanding of the environmental conditions that sustain the remarkable carbon density of high-elevation forests in the region. We hypothesize that forest AGB is highest in terrain units where the availability of biologically usable water, defined here as the portion of soil moisture accessible to vegetation<sup>42</sup>, shaped by both topographic water accumulation and atmospheric moisture demand is maximised while the likelihood of damaging disturbance events such as avalanches is minimised.

The overarching aim of this study is to understand how fine-scale topoclimatic variation influences the distribution of forest AGB in high-elevation regions of the Central Himalayas. Our specific objectives were to: (1) identify the topographic conditions associated with high AGB forests, (2) evaluate the role of terrain-modulated water and energy availability in shaping spatial variation in AGB, and (3) assess the extent to which disturbance-related terrain factors constrain forest biomass below its potential. These objectives are addressed through three interconnected hypotheses that guide our analysis: (1) High forest AGB is associated with specific terrain units, defined as areas characterized by distinct combinations of terrain attributes such as elevation, slope, topographic position, and exposure, (2) Forest AGB increases with the availability of biologically usable water, which is modulated by interactions between climate and topographic position, and (3) Forest AGB is constrained below its topoclimatic potential as the likelihood of disturbances, such as avalanches and mass movements, increases, with these disturbances being strongly influenced by topography. Our findings contribute to improved forest carbon modeling in complex topoclimatic regions and inform strategies for carbon conservation in climate-sensitive mountain ecosystems.

## Materials and methods

### *Study area*

The study area comprises the country of Nepal (147,516 km<sup>2</sup>) in the Central Himalayas. It has a remarkable elevational gradient from less than 100 m a.s.l. in the southern lowlands to over 8,000 m a.s.l. in the High Himalayas, encompassing one of the steepest and most ecologically diverse vertical transects globally. This sharp relief, combined with complex topoclimatic conditions, gives rise to a wide range of forest types across short spatial distances ranging from subtropical broadleaf forests in the southern plains to sub-alpine coniferous forests dominated near the treeline<sup>43</sup>. This ecological diversity provides an ideal setting to examine how fine-scale topoclimatic variability influences forest structure and biomass distribution in mountainous terrain.

### *Plot level forest inventory data*

We used a comprehensive georeferenced dataset of 2,009 plot-level estimates AGB (tonnes per hectare, t ha<sup>-1</sup>), derived from Nepal's 2010–2014 national forest inventory. Plot-level AGB was estimated from tree measurements using allometric equations. The dataset along with a detailed description, is available in<sup>41</sup>. In this study, we use AGB as a proxy for forest productivity and carbon storage, given its central role in ecosystem functioning and responsiveness to environmental gradients. The nationally consistent and spatially extensive dataset is particularly valuable for capturing the high variability of biomass across Nepal's heterogeneous mountain forests, where climatic, edaphic, and disturbance factors interact across scales.

### *Terrain analysis*

We conducted a two-step digital terrain analysis to test hypothesis 1, that carbon dense forests occur preferentially in specific terrain units. First, image segmentation based on a set of topographic attributes (Table 1) that was shown to be associated with variation in forest carbon pools<sup>31</sup>, was used to delineate contiguous, homogeneous terrain units. Principal components analysis (PCA) was performed on the terrain attributes

Attributes	Description	Unit
Elevation	Digital Elevation Model (DEM) from ASTER <sup>44</sup> . It influences forest carbon storage, primarily by affecting temperature, precipitation, soil depth and human disturbance <sup>31</sup>	m a.s.l.
Slope	The slope gradient of terrain derived from the DEM. Slope, in conjunction with elevation, modulates forest carbon through its effects on temperature, precipitation, and soil properties	degree
Plan Curvature	The curvature in the horizontal plane of the contour line <sup>45</sup> . Flows concentrate on concave surfaces and disperse on convex ones, affecting erosion patterns <sup>46</sup>	m <sup>-1</sup>
Profile Curvature	The curvature in the vertical plane of a flow line <sup>45</sup> . Affect soil moisture by increasing water flow speed on convex surfaces and decreasing on concave ones which tend to be depositional environments <sup>46</sup>	m <sup>-1</sup>
Topographic Wetness Index (TWI)	A high TWI indicates higher water accumulation potential, through a combination of relatively low slope gradient and large contributing drainage area. Steep, well-drained, slopes are relatively dry and have low TWI values <sup>47</sup>	–
Potential insolation (PISR)	DEM derived potential incoming solar radiation using a lumped Atmospheric Transmittance model of monthly insolation at 5-days and 0.5-hour steps for a year <sup>48</sup> . Solar radiation contributes to spatial variation in forest carbon by modulating microclimatic conditions and driving differences in forest productivity	kWh m <sup>-2</sup>
Vertical distance to channel network	The vertical height above the interpolated channel network. Indicates the distance of a grid cell from the groundwater <sup>49</sup> . It serves as a proxy for a proximity to groundwater and drainage dynamics	m
Slope Length and Steepness factor (LSF)	Combines S-factor (steepness) and the L-factor (length). Also referred to as the sediment transport capacity index <sup>47</sup> and used as an input in the Revised Universal Soil Loss Equation (RUSLE) <sup>50</sup>	–
Topographic position index (TPI)	The TPI compares the elevation of each grid cell to the mean elevation of a specified neighbourhood around that cell. Here, a 100 m diameter circular neighbourhood was used. Positive values are typical of ridges, negative values in valleys and near-zero values in flat areas <sup>51</sup>	–
Wind exposure	The average 'Wind Effect Index' for all directions using an angular step. A dimensionless index. Values<1 signify leeward areas, while values>1 indicate windward areas <sup>48</sup> . It influence mechanical stress, evapotranspiration rates, and disturbance intensity—factors that shape biomass accumulation and retention	–

**Table 1.** Topographic attributes with a spatial resolution of 30 m, derived from a digital elevation model using SAGA-GIS<sup>49</sup>.

and image segmentation applied on outputs to derive terrain units with homogeneous topographic attributes. Details on terrain analysis, including segmentation parameters, algorithms, and software tools, are presented in supplementary information S.1.1.2. Then, for terrain units that included plot-based forest AGB estimates (N = 519), we compared topographic attribute distributions of forests with high or low AGB.

Our study focused on high-elevation forests, here defined as forests located above 1516 m a.s.l.; the elevation threshold of 1516 m a.s.l. was based on a breakpoint in the distribution of forest AGB by elevation (<sup>4</sup> and supplementary information Figure S1).

High AGB forest plots were defined as those within the top 10% of all plot observations<sup>41</sup> from the high elevation zone (>1516 m a.s.l.); corresponding to 90<sup>th</sup> percentile cut-off value (>531 t ha<sup>-1</sup>). Using this AGB threshold, all forest inventory plots>1516 m a.s.l. (N = 835) were categorized as either 'high AGB density' (>531 t ha<sup>-1</sup>) or 'low AGB density' (≤ 531 t ha<sup>-1</sup>). To address within-segment variations, terrain units with at least one inventory plot exceeding the AGB threshold were assigned to the high AGB forest class. Terrain units derived from multivariate topographic clustering were assumed to exhibit internal biophysical homogeneity; therefore, the occurrence of a high AGB plot within a unit was taken as indicative of conditions favourable to elevated biomass. The reclassified subset comprised 835 plots distributed across 519 terrain units, with 65 and 454 classified as high and low AGB forest, respectively. Subsequently, a Mann-Whitney U Test with effect size measures was employed to assess significant differences in topographic attributes between terrain units of high and low forest AGB. Due to the unequal distribution of sample sizes across forest biomass classes, the non-parametric nature of the Mann-Whitney U Test made it suitable for comparing terrain and climatic variables between these groups. Further methodological details, including preprocessing workflows, variable preparation, model fitting procedures, and diagnostics, are provided in Supplementary Information S1.1.

*Topoclimatic gradient analysis*

To test hypothesis 2, we characterized fine-scale variations in water and energy availability, and then analysed the relationship with forest AGB. A modified topographic wetness index, computed from a digital elevation model and gridded mean monthly precipitation data, was used as an indicator of water availability, while mean monthly potential evapotranspiration was modelled with the modified Hargreaves-Samani equation and used as an indicator of energy availability.

**a) Modified topographic wetness index** In mountainous landscapes, water from precipitation is potentially redistributed along slopes and within catchments as a function of topographic relief and the hydrological properties of the (sub)surface. Terrain units that are excessively drained, such as steep upslopes with thin soils, typically lose water and sediment through runoff and erosion, while footslopes and valleys with deeper soils may receive lateral water inputs from the upslope areas. These redistribution processes may produce pronounced spatial variation in soil water availability and vegetation cover, especially in semiarid landscapes where ridges and upslopes are typically sparsely vegetated while footslopes and gullies support more dense vegetation cover<sup>52</sup>.

The Topographic Wetness Index (TWI)<sup>53</sup> is commonly used to capture topography-driven variation in potential water availability<sup>54</sup>. The TWI was developed to model the likelihood of saturation-excess overland flow across the landscape as a function of local slope gradient and upslope drainage area (Eq. (1)):

$$TWI = \ln(\alpha/\tan\beta) \quad (1)$$

where,  $\alpha$  = Specific upslope drainage area with dimension  $\text{m}^2 \text{m}^{-1}$  of contour line and  $\beta$  = Topographic slope gradient in radians.

The TWI is based on the implicit assumption that precipitation and soil hydrological properties are spatially homogeneous, which may apply within a small catchment or landscape but does not hold across large climatically diverse territories like the Central Himalayas. Since detailed soil hydrological information is not available for Nepal, while gridded mean monthly climate data is available, one option to account for some of the broad-scale climate variation in the TWI is to incorporate a term that depends on monthly precipitation.

We assumed that: i) topography-driven redistribution of water is negligible in landscapes of the most arid climate zones, ii) maximised in landscapes of the wettest climate zones, and iii) is captured by the TWI within a given climate zone. To represent the assumed effect of climate aridity on the potential for water redistribution we modified the TWI (termed as scaled TWI) by adding a linear ramp function, such that the potential for water redistribution becomes zero for arid landscapes and maximal in the wettest landscapes (Eqs. (2) and 3):

$$STWI = \sum_{i=1}^{12} \ln(f \cdot \alpha/\tan\beta) \quad (2)$$

$$f = \begin{cases} 0, & P < P_{\min} \\ 1, & P = P_{\max} \\ cP, & P_{\min} \leq P < P_{\max} \end{cases} \quad (3)$$

where,  $\alpha$  = specific upslope drainage area with dimension  $\text{m}^2 \text{m}^{-1}$  of contour line,  $\beta$  = topographic slope gradient in radians,  $P$  is mean monthly precipitation ( $\text{mm month}^{-1}$ ), computed as the sum of mean monthly rainfall (MMR)<sup>55</sup> and snow water equivalent (SWE)<sup>56</sup>,  $P_{\min}$  is the minimum mean monthly precipitation for topography-driven water redistribution to occur,  $P_{\max}$  is the mean monthly precipitation at which topography-driven water redistribution is assumed to be maximal, and  $c$  is the slope of the ramp function  $f$ . The parameters  $P_{\min}$ ,  $P_{\max}$  and  $c$  were arbitrarily set at  $100 \text{ mm month}^{-1}$ ,  $500 \text{ mm month}^{-1}$  and  $0.002$ , respectively. The  $P_{\max}$  value of  $500 \text{ mm month}^{-1}$  corresponds to the 95<sup>th</sup> percentile  $P$  value of the national forest inventory plots. Upslope drainage area and slope gradient rasters were derived from the DEM using SAGA-GIS<sup>49</sup>.

**b) Potential Evapotranspiration (PET)** The modified Hargreaves and Samani equation<sup>57</sup> was used to predict mean monthly PET (Eq. 4). This model is recommended for areas of limited data availability<sup>58</sup>, as it predicts PET from just two commonly available variables, extraterrestrial radiation and monthly air temperature.

$$PET = 0.0135(K)(R_a)(T_{\max} - T_{\min})^{0.5}(T + 17.8) \quad (4)$$

where,  $T_{\max}$  = maximum monthly air temperature ( $^{\circ}\text{C}$ ),  $T_{\min}$  = minimum monthly air temperature ( $^{\circ}\text{C}$ ),  $T$  = mean monthly air temperature ( $^{\circ}\text{C}$ ),  $R_a$  = extraterrestrial radiation ( $\text{mm day}^{-1}$ ),  $K$  = empirical coefficient.  $K$  relates global solar radiation to differences in the range of daily temperature. Calculation details for  $T_{\max}$ ,  $T_{\min}$ ,  $T$ ,  $R_a$  are provided in the supplementary information S1.1.

Exploratory data analysis revealed parabolic relationships between forest AGB and STWI and PET (Fig. 2), rendering linear models unsuitable. Consequently, Generalised Additive Models (GAMs) were deemed appropriate to capture these complex relationships by fitting nonlinear smooth functions<sup>59</sup>. Quantile regression using the 'qgam' package<sup>60</sup> was implemented to model maximum forest AGB for a given combination of STWI and PET, with quantiles estimated at  $\tau = 0.99$ , assuming joint constraints of energy and water availability on forest AGB in a nonlinear way (Eqs. 5 and 6). Tensor product smooths (te) were used to model the interaction between covariates, measured in different units<sup>59</sup>. We employed the 'check.qgam' function from the 'qgam' package to inspect the fitted model and validated it using binning and a leave-one-out approach.

$$AGB \sim s(STWI) + s(PET) + ti(STWI, PET) \quad (5)$$

$$AGB \sim te(STWI, PET) \quad (6)$$

where STWI is the Scaled Topographic Wetness Index, PET is potential evapotranspiration ( $\text{mm day}^{-1}$ ) and  $s$ ,  $te$  and  $ti$  are tensor product smooth functions.

To test hypothesis 3, we compared the statistical distributions of topographic attributes that are indicative of the likelihood of erosion, avalanches and mass movements, for terrain units having high or low AGB forest.

## Results

### Terrain analysis

High AGB forests were found to occur in distinct topographic positions compared to low AGB forests as the distributions of several terrain attributes significantly differed between high and low AGB forest (Fig. 1). The Mann-Whitney U test indicated significant differences in median values for elevation, topographic position index (TPI), and wind exposure between the two groups. While low AGB forests occurred across a wide range of habitats, high AGB forests were more restricted, indicating their association with specific topographic positions or terrain units. Rank-biserial correlation ( $\hat{r}$ ), ranging from  $-1$  to  $+1$ , indicates the strength and direction of the association between the ranked variables<sup>61</sup>. Positive  $\hat{r}$  were observed for elevation, plan curvature, profile curvature, TPI, vertical distance to the channel, slope, and wind exposure, indicating that

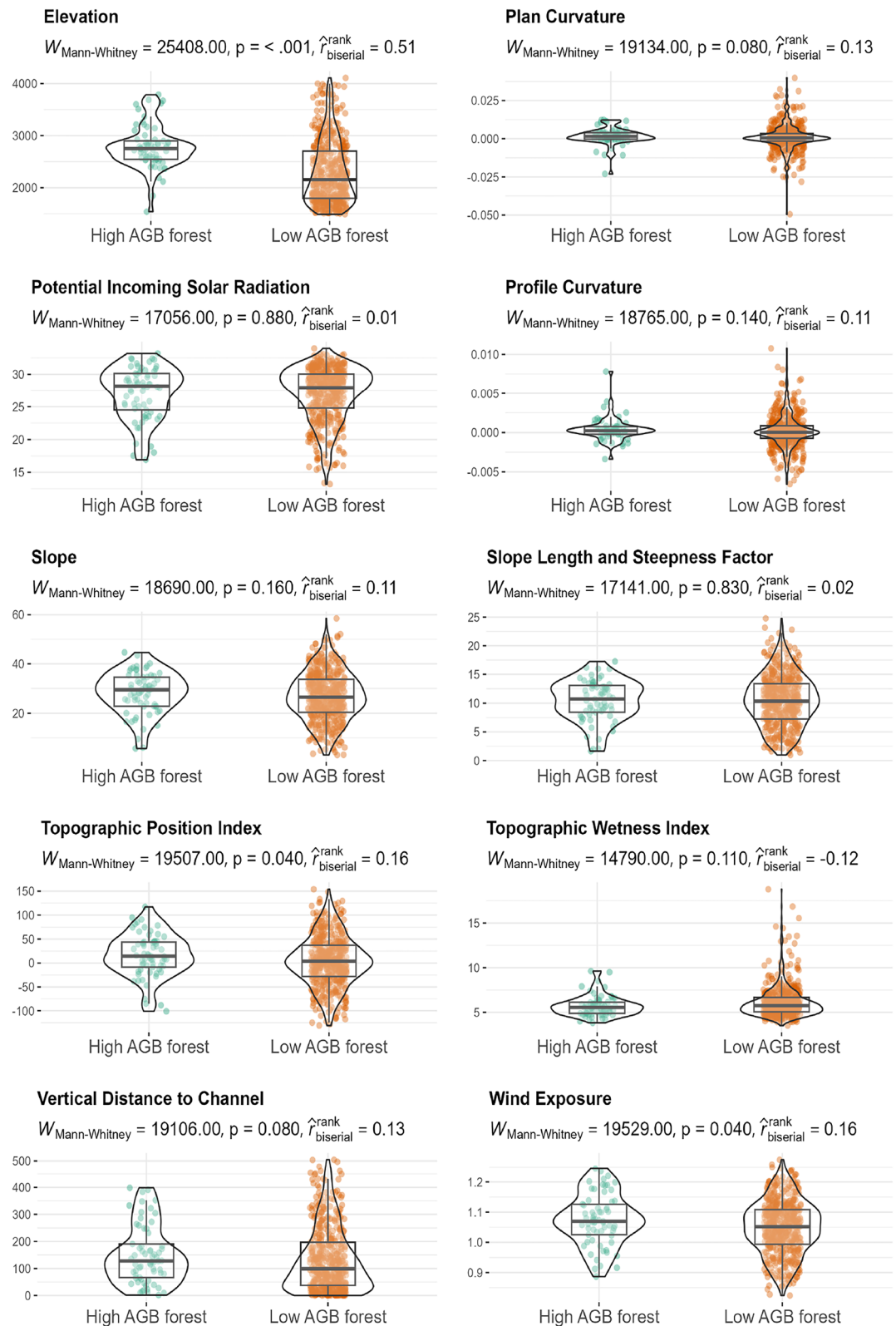


**Figure 1.** Comparison of distributions of terrain attributes for terrain units having high AGB (green) and low AGB forest (orange). The subheading of each figure shows the test statistic, p-value and rank-biserial correlation for Mann-Whitney U Test.



terrain units containing high AGB forests tended to have larger values of these terrain attributes compared to terrain units without high AGB forests. Conversely, the topographic wetness index (TWI) had a negative  $\hat{r}$ , being higher in terrain units without high AGB forests. For slope length and steepness factor (LSF) and potential incoming solar radiation (PISR),  $\hat{r}$  values were marginal. These findings support hypothesis 1, suggesting that high AGB forests are consistently associated with topographic settings that offer both shelter and favourable microclimatic conditions. In contrast, low AGB forests occurred across a broader range of habitats, indicating weaker environmental filtering.

#### Topoclimatic gradient analysis.

Forest AGB exhibited a parabolic relationship with topographic indicators of climatic water and energy availability, supporting hypothesis 2. Specifically, the highest AGB values were observed in areas characterized by a combination of relatively high STWI and PET (Fig. 2, Supplementary information Figure S3). This parabolic pattern was confirmed using nonparametric quantile regression with B-splines, which showed peak AGB occurring near the 95<sup>th</sup> and 99<sup>th</sup> quantiles of STWI and PET. These findings indicate that forest productivity is optimized under moderate-to-high topoclimatic moisture and energy conditions, beyond which further increases in water or energy availability do not correspond to higher AGB.

To further investigate the relationship between forest AGB and topographic indicators of climatic water and energy availability, we conducted a topoclimatic gradient analysis using quantile GAM (QGAM) modelling. We focused on the maximum forest AGB ( $\tau = 0.99$ ) across the range of climatic energy and water availability in the data set (supplementary information Figure S4). The response surface depicted the variation in predicted maximum forest AGB with STWI and PET (Fig. 3). The result show that the 99<sup>th</sup> quantile of forest AGB was responsive to the interaction between STWI and PET, predominantly concentrated along the anti-diagonal of the covariate-space. These findings demonstrate that forest AGB increases with the interaction of STWI and PET, which are proxies for biologically usable water availability.

Comparison of the two models, namely the 'main plus interaction' and 'interaction only' (Eqs. 5 and 6), showed that while the 'main plus interaction' model improved the fit, it required additional parameters (Supplementary information Table S1, S2 and S3). Therefore, the 'interaction only' model was considered a more straightforward choice for modelling forest AGB, accounting for the expected interaction between STWI and PET.

The 'interaction only' model (Eq. 6) demonstrated reasonable accuracy in predicting extreme forest AGB, as shown by the strong positive relationship between observed and predicted values (Fig. 4). However, the

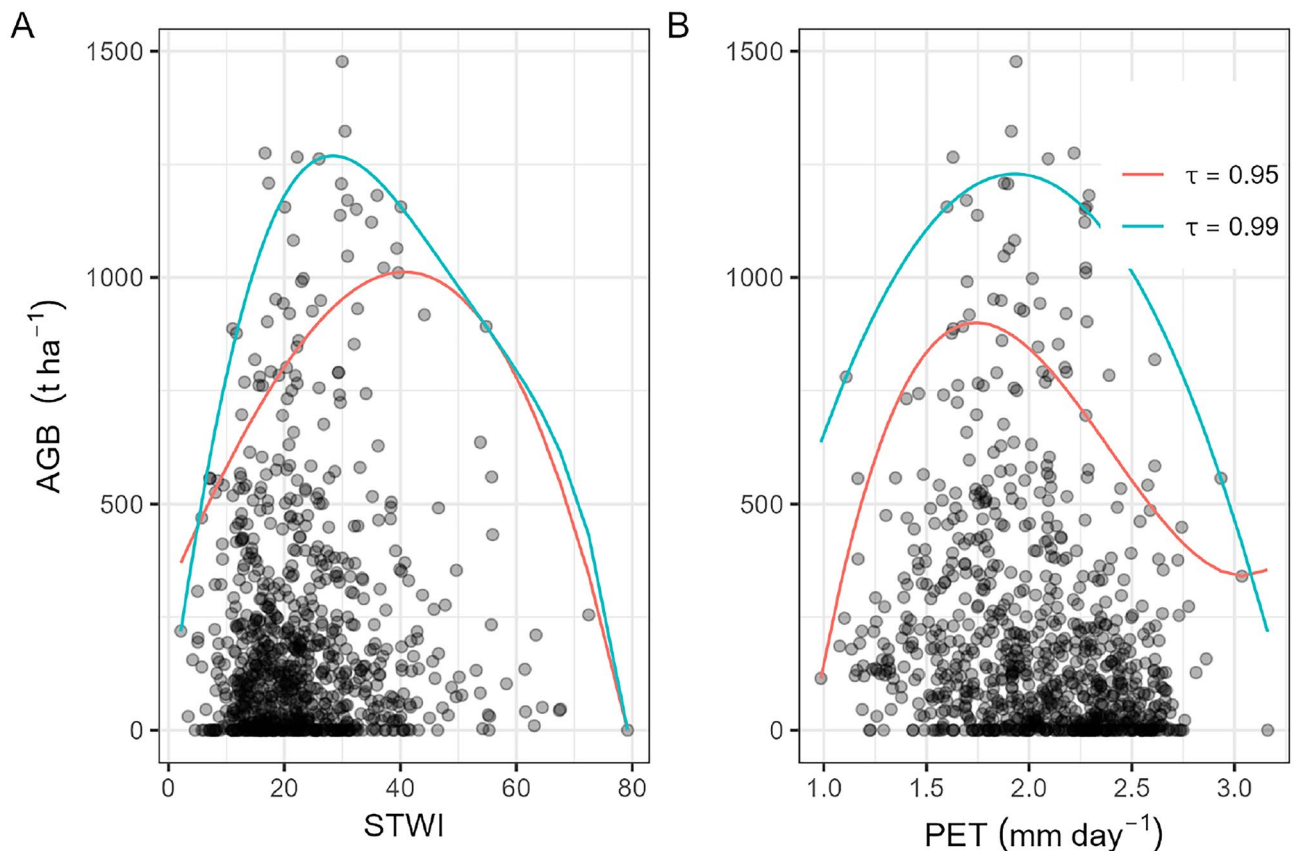


**Figure 2.** A nonparametric quantile regression using B-splines to explore the 95<sup>th</sup> ( $\tau = 0.95$ ) and 99<sup>th</sup> ( $\tau = 0.99$ ) quantiles of the conditional distribution. Panels (A) and (B) fit forest AGB as a function of scaled topographic wetness index (STWI) and mean daily potential evapotranspiration (PET), respectively.

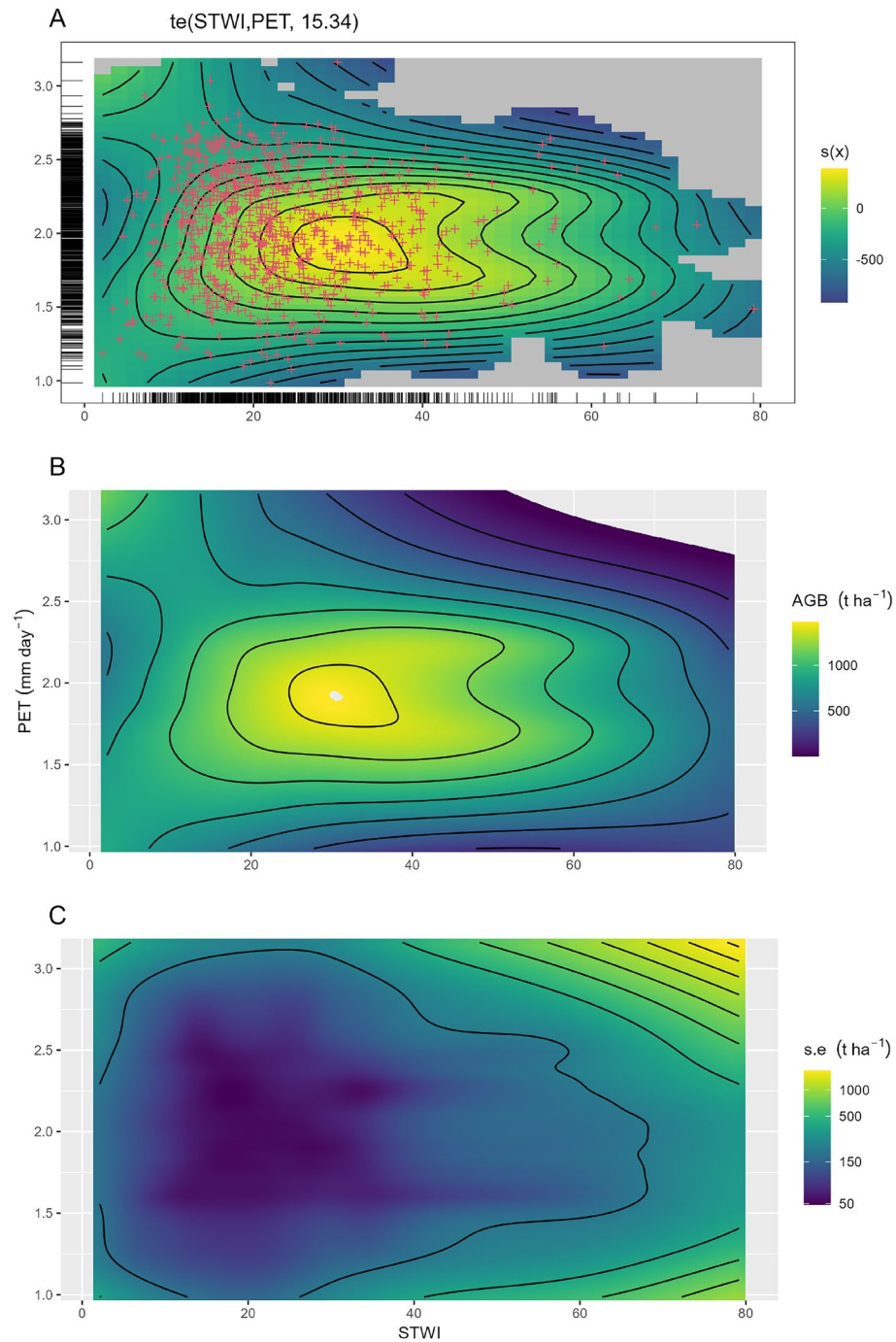


**Figure 3.** The contour plot (Panel A) of the smoothed function  $s(x)$  shows the estimated relationship between the response and predictor variables. The colour intensity indicates the magnitude of the predicted response at different combinations of predictor variables. The term ‘te’ stands for tensor product smooth function, which is used to model the joint effect of the predictors with an effective degrees of freedom of 15.34. The red + symbols represent input data points for the model, while grey areas represent no data area. Panel (B) shows the predicted 99<sup>th</sup> quantile AGB with the fitted QGAM. The se contour surface plot (Panel C) shows the estimated standard errors of the predicted forest AGB for different combinations of the predictor variables.

agreement between observed and predicted AGB varied depending on the data binning approach, with a trade-off between bin count and the number of forest inventory plots per bin. Validation using nine bins revealed the lowest Root Mean Square Error (RMSE) for predicted forest AGB at  $\tau = 0.99$ . This RMSE variability among bins is attributed to the distribution of inventory plots across climatic space (STWI and PET), with fewer plots at the extremes and more toward the center.

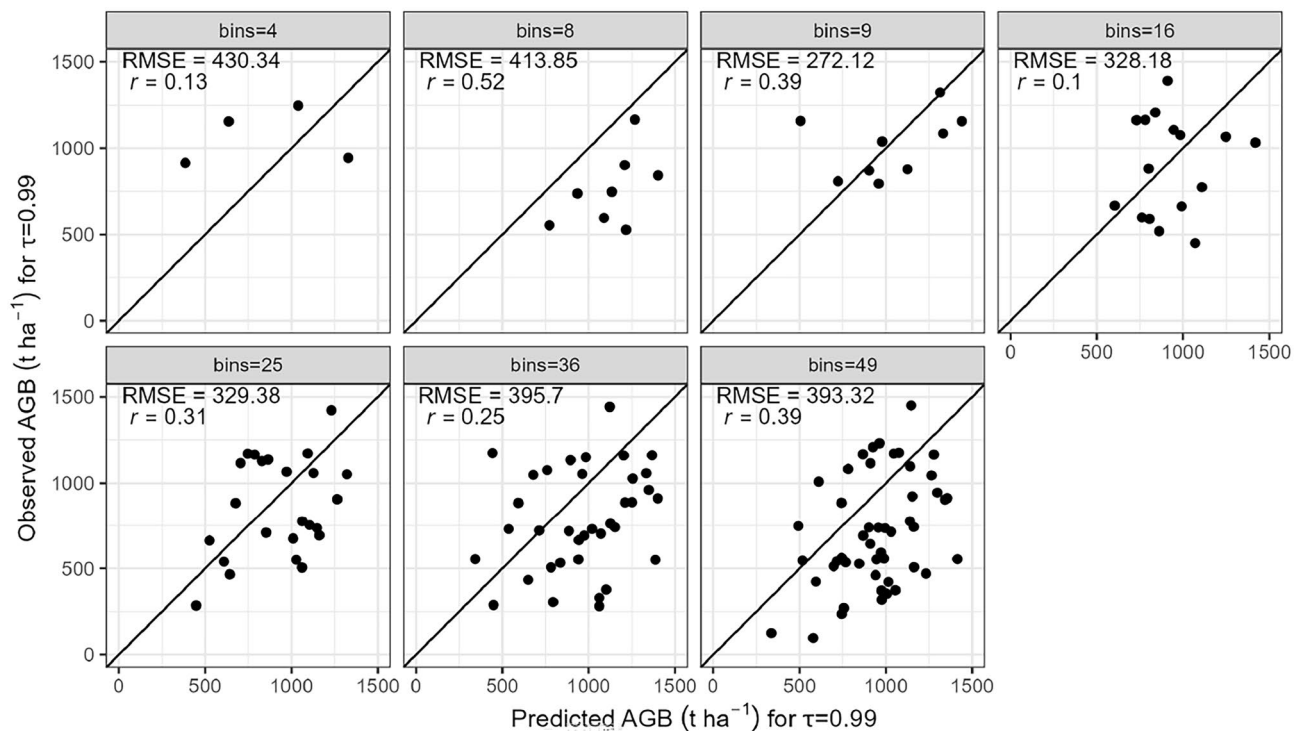


**Figure 4.** The observed and predicted maximum forest AGB using ‘interaction only’ quantile GAM at  $\tau = 0.99$  for forest inventory plots belonging to different bins of the surface of scaled topographic wetness index (STWI) and potential evapotranspiration (PET). The RMSE and Pearson correlation coefficient ( $r$ ) compare observed and predicted values. The dots compare the observed and predicted maximum forest AGB for each bin, with RMSE estimated using the leave-one-bin-out method.

We hypothesised (H3) that forest AGB is constrained below its topoclimatic potential where the likelihood of disturbances, such as avalanches and mass movements, is relatively high. To evaluate this hypothesis, we compared the statistical distributions of topographic attributes, indicative of disturbance likelihood, before and beyond the observed AGB maximum. The analysis revealed that AGB peaks at a PET value of approximately  $2 \text{ mm day}^{-1}$  (Fig. 5) and an STWI value just under 40 (Supplementary information Figure S2). Beyond these thresholds, a decline in AGB was observed. However, this decrease is less certain due to the low density of data points in regions with higher STWI and PET values, particularly for the STWI. The observed decline in AGB at higher STWI ( $> \sim 40$ ) and PET ( $> \sim 2 \text{ mm day}^{-1}$ ) values raises questions about underlying mechanisms. We hypothesize that this reduction is driven by increased levels of disturbance, such as erosion, avalanches, and mass movements, which may become more frequent or severe in areas with these environmental conditions. The basis for this conclusion is the significant differences in the basic terrain attributes indicating proxies of disturbance likelihood both human induced as well as natural.

## Discussion

Building on previous findings that showed the mediating role of terrain on forest carbon stocks through its effects on climate and disturbances at a fine scale in the Central Himalayas<sup>31</sup>, we aimed to explore in greater detail how these fine-scale terrain variables influence the availability of climatic water and energy, thereby affecting the distribution of forest carbon. We explored relationships between forest biomass patterns and topographic positions indicative of potential forest growth conditions<sup>4</sup>. Specifically, we demonstrated that the most carbon-dense forests are associated with distinct topographic settings that likely provide shelter and favourable microclimatic conditions, while carbon storage is reduced below the topoclimatically constrained potential in areas prone to disturbances such as avalanches and mass movements (Hypothesis 1). Our findings confirm the hypothesized role of topoclimatic factors in shaping forest AGB patterns in high mountain forests of Nepal (Hypothesis 2). These findings reaffirm the significant influence of fine-scale topographic heterogeneity on climatic variability<sup>62</sup> and forest structure and carbon density<sup>63</sup>.

High AGB forests were predominantly found on ridgetops and upper slopes, characterized by relatively high Topographic Position Index (TPI) values. Forest inventory plots with high AGB were associated with TPI values close to zero, whereas plots of low AGB forests exhibited a broader range of TPI values. This pattern contrasts with findings from areas of lesser topographic complexity, where high AGB forests are more commonly found on flat terrain<sup>64</sup>, where the risk of soil erosion and mass movements like avalanches and landslides is minimized. Moreover, sites with high wind exposure are generally drier due to enhanced evapotranspiration<sup>65</sup>. However, our study in the Central Himalayas indicates that windward slopes can also be notably wet due to increased precipitation from orographic uplift compared to leeward slopes<sup>35</sup>. This elevation in moisture can counteract



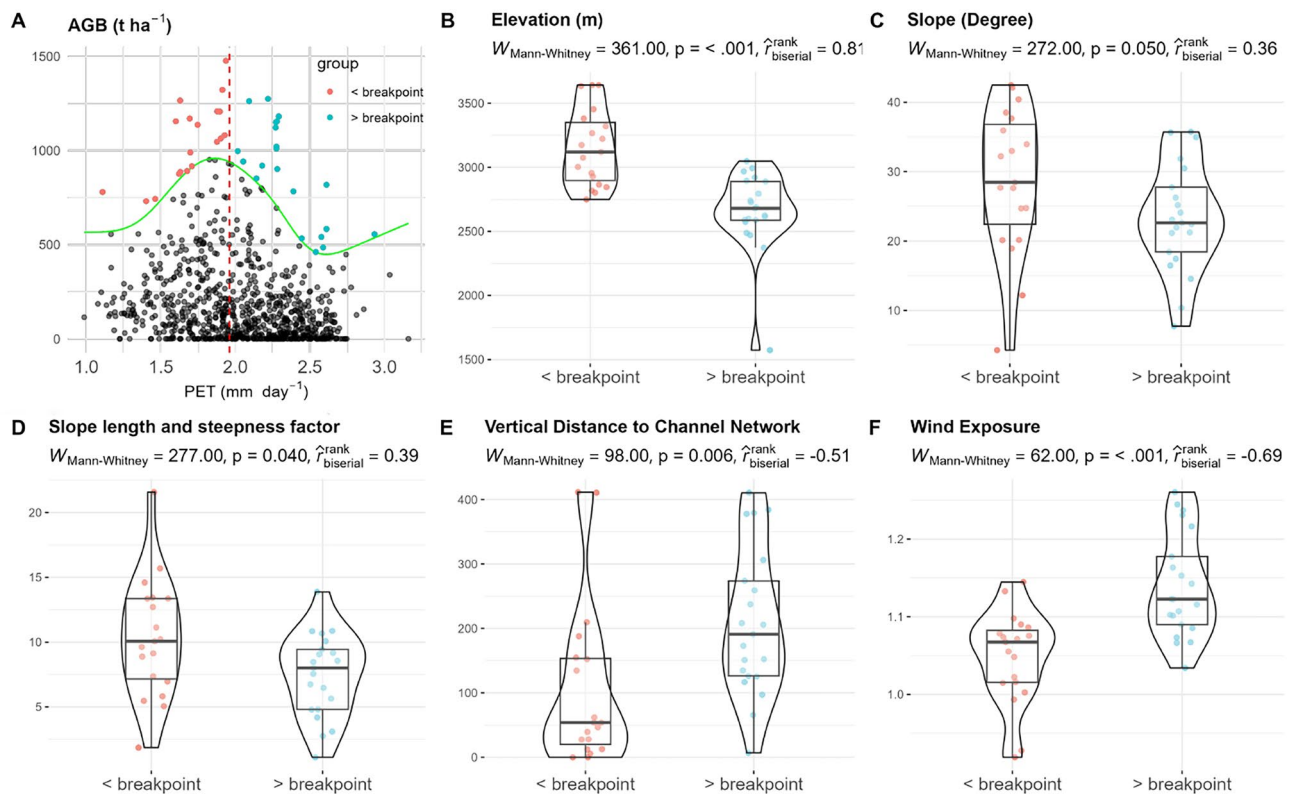


**Figure 5.** Grouping of forest inventory plots based on the breakpoint detected (1.88) in potential evapotranspiration (PET) at the high quantile ( $\tau = 0.95$ ). The breakpoint is indicated by the dashed red line (Panel A). The solid green line represents the fitted quantile gam ( $\tau = 0.95$ ). Red and blue points represent inventory plots categorized as below and above the PET breakpoint, comprising 46% and 54% of the total plots above fitted quantile, respectively. Panels (B–F) compare common terrain attributes for inventory plots below and above the PET breakpoint. The subheading of each panel shows the test statistic, p-value, and rank-biserial correlation coefficient from the Mann–Whitney U test.

the drying effect, supporting the growth of taller, more robust forest stands<sup>66</sup>. These findings emphasize the significant role of topographic variability in determining forest structure and carbon density, underscoring the critical influence of fine-scale environmental heterogeneity in shaping forest habitats.

The comparison of plan and profile curvature, quantifying surface convexity or concavity in horizontal and vertical planes, respectively<sup>47</sup>, revealed weak but positive associations with high forest AGB occurrence. Rank-biserial correlation coefficients for plan and profile curvature were 0.13 and 0.11, respectively, and although Mann–Whitney U-tests yielded non-significant p-values, the direction of effect suggests a tendency for high AGB forests to occur in terrain units with positive curvature values. Specifically, positive plan curvature indicates convex features in the horizontal plane (ridges), while positive profile curvature denotes concave shapes in the vertical plane (concave slope forms in depositional environments)<sup>47,67</sup>. While convex planforms are not typically associated with moisture accumulation due to increased runoff and lower sediment retention<sup>68,69</sup>, they may confer reduced exposure to disturbance processes such as avalanches and mass movements, which are more frequent in concave hollows or convergent flow paths<sup>70</sup>. Thus, the association between positive curvature and high AGB may reflect the interaction between favourable microsite stability and reduced disturbance exposure, rather than water availability alone.

High AGB forests were typically found at a greater vertical distance from the nearest stream channels and exhibited lower TWI values compared to low AGB forests. This suggests that highly productive forests in mountainous terrain are not necessarily found in the wettest or most hydrologically convergent locations. In contrast, low AGB forests were more frequently associated with higher TWI values, indicative of their occurrence in areas with increased proximity to water bodies or major flow pathways. While TWI is commonly used to infer drainage potential and moisture availability<sup>53,71</sup>, these findings suggest that excess water accumulation may not always favour biomass accumulation, possibly due to increased susceptibility to disturbance processes such as landslides or saturation-induced root instability in concave or poorly drained areas. This interpretation is supported by the observed terrain context of high AGB forests, which tend to occur on positions with lower disturbance exposure, such as convex planforms and areas with greater vertical separation from major drainage lines. These positions may offer more stable substrates, enabling long-term biomass accumulation despite lower apparent water availability. Thus, in our high mountain study area, the association of topographic position with

disturbance regimes may be more critical to sustaining high forest carbon density than terrain-driven variation in resource availability.

Other terrain attributes, such as the slope length and steepness factor (LSF) and potential incoming solar radiation (PISR), did not significantly differ between high and low AGB forest plots. Despite the theoretical expectation that low LSF values are associated with reduced erosion and potentially deeper soil development<sup>72</sup>, our results suggest that forest productivity is not strongly constrained by slope length alone in this context. Similarly, although PISR influences energy availability and growing season length, the absence of strong differences between AGB classes indicates that topographic variation in insolation may be less limiting than soil moisture or disturbance-related factors in determining carbon density at the scale examined.

We examined topoclimatic variation in forest site productivity using Scaled Topographic Wetness Index (STWI) and potential evapotranspiration (PET) as proxies for climatic water and energy availability. Our analysis has shown that the probability of finding high AGB forest increases with the interaction of PET and STWI to a maximum at intermediate PET and STWI, consistent with forest productivity being highest where biologically usable water and energy are maximized<sup>30</sup>. Our findings reveal that the upper quantiles of AGB exhibit a humped relationship with PET and STWI, with an AGB maximum observed at PET of approximately 2 mm day<sup>-1</sup> and STWI of approximately 30. These results align with our hypothesized association between AGB and biologically usable water. Contour plots (Fig. 3) illustrated the sensitivity of predicted forest AGB and the interaction effect size to PET and STWI, highlighting their significant influence on forest AGB. This pattern aligns with established knowledge of energy and water constraints in determining productivity patterns at a broad scale<sup>42</sup>. Nevertheless, a weak declining trend in forest biomass for sites with highest STWI and PET contrasts with expected effects but could not be confirmed due to limited observations and higher model standard error (Fig. 3C).

Comparing the smooth effect of AGB with STWI, Topographic Wetness Index (TWI), and mean annual rainfall (supplementary information Figure S6), STWI exhibited a more stable estimate than rainfall, while TWI failed to capture the AGB variability. The stronger relationship between STWI and AGB suggests that STWI better represents spatial variation in water availability in mountainous landscapes by integrating topography and seasonal rainfall. This is supported by lower AIC values (supplementary information Table S4 and Figure S5), and aligns with observations that incorporating topography improves fine-scale soil moisture characterization<sup>73</sup>. However, it is important to note that the linear ramp function used to rescale the wetness index relies on the basic assumption of water redistribution, which may not fully capture the complexities present in areas with highly heterogeneous topoclimate. To address this limitation, we recommend future research that incorporates inputs related to soil attributes, terrain characteristics, precipitation patterns, and vegetation properties.

The AGB response surface showed a humped relationship with PET, used as a proxy for climatic energy availability. Consistent with observations in other mountainous regions<sup>74</sup> including the reported range of values for Nepal Himalayas<sup>75,76</sup>, the elevational pattern of PET showed declining maximum values at higher elevations, which reflects elevational gradients of increasing radiation and wind speeds, and decreasing air temperature and humidity. The extreme PET values (>2.5 mm day<sup>-1</sup>) at higher elevations in the Central Himalayas correspond to arid environments<sup>77</sup> that can only sustain low-stature vegetation with low AGB (<500 t ha<sup>-1</sup>). However, high AGB forest can persist at moderate PET (1.5–2.5 mm day<sup>-1</sup>) in these mountain ranges, which is likely related to snow cover. Snow cover may affect this finding in two ways. Firstly because our estimates of mean annual PET were based on the modified Hargreaves method that primarily captures air temperature and radiation effects, and may overestimate PET, especially in arid mountain landscapes with significant snow cover<sup>78</sup>. Secondly, snow cover may add significant amounts of moisture to the soil during snow melt that allows the forest to meet high atmospheric moisture demand during periods of low precipitation.

To further investigate the observed patterns and test hypothesis 3, we analysed the statistical distributions of topographic attributes indicative of disturbance likelihood across breakpoints in the proxies of climatic water availability, comparing areas with high and low AGB classes. Our analysis of terrain attributes revealed contrasting relationships between aboveground biomass (AGB) and proxies for biologically usable water availability across inventory plots. Plots with lower AGB on higher PET were located at significantly lower elevations with gentler slopes and smaller slope length and steepness factor (LSF). However, these same plots had a greater vertical distance to the channel network and higher wind exposure. Intuitively, one might expect that sites with greater susceptibility to disturbances, such as erosion and mass movements, would align with high PET. For instance, steeper slopes in mountainous regions are prone to events like avalanches<sup>79</sup> and rockfalls<sup>32</sup>. These disturbances can significantly affect forest structure, including stem density per hectare<sup>80</sup>. However, our findings do not align with this expectation. Two key factors contribute to these contrasting results. Firstly, our inventory plots were measured based on physical accessibility. Consequently, steeper forests with low biomass may not have been adequately sampled in the high elevation plots originally designed. Secondly, the regions exhibiting relatively higher PET but low maximum forest AGB predominantly represent stands occurring above 2500 meters above sea level (m a.s.l.). Forest stands at lower elevations have experienced a history of intense human disturbance<sup>81</sup>, contributing to their overall lower AGB compared to both lower sub-tropical regions and higher altitude zones. This disparity may, in part, reflect reduced anthropogenic pressure in rugged, high-altitude areas, in contrast to the more accessible lowland forests that typically support higher population densities<sup>82</sup>. Thus, we can expect higher disturbance to forest due to the combined effect of higher mean annual precipitation<sup>83,84</sup> and human induced disturbance such as road construction is the major factor for slope failures<sup>85</sup>. The maximum forest AGB in Nepal around 3000 m a.s.l. has been attributed to the presence of stands characterized by high stand density, large-diameter trees, and species with high wood density<sup>4</sup>.

Moving beyond slope, elevation, and the steepness factor (LSF), we explore the relationship of forest AGB with vertical distance to the channel network and wind exposure. Interestingly, for the group of plots showing a negative relationship between AGB and PET, the higher vertical distance to the channel network suggests potentially decreased access to moisture. This, in turn, enhances soil quality and depth<sup>86–88</sup>. Additionally, wind

exposure plays a role, whether by promoting seedling regeneration or influencing forest structure dynamics by influencing regeneration and establishment of seedlings<sup>89</sup>, physical damage of trees<sup>90</sup>, or even contributing to burn severity. Our findings underscore the complexity of AGB-PET interactions, influenced by terrain attributes, elevation, and likelihood of disturbance.

## Conclusion

We aimed to identify how fine-scale topoclimatic variation influences environmental conditions that sustain high levels of forest AGB across the rugged landscape of the Central Himalayas. Our findings demonstrate that high AGB forests are consistently associated with distinct terrain units where both climatic energy and biologically usable water are elevated. These topographic settings appear to offer stable environmental conditions conducive to long-term forest carbon accumulation. In contrast, areas with higher disturbance potential, despite sometimes greater resource availability, tend to support lower forest AGB. Our study highlights the importance of landscape heterogeneity in shaping spatial patterns of forest carbon density. These insights contribute to improved understanding of carbon storage dynamics in mountainous ecosystems and underscore the need to account for fine-scale terrain variation in forest carbon assessments and management planning. We recommend that future biomass estimation and conservation efforts in mountain regions incorporate high-resolution topoclimatic, vegetation and terrain data to better identify and protect forest areas with high carbon storage potential. Additionally, prioritizing topographic positions that are well protected in forest management could enhance the long-term stability of forest carbon stocks under changing climate and disturbance regimes.

## Data availability

Forest AGB data for each plot is available on Figshare repository (<https://doi.org/10.6084/m9.figshare.21959636>). The topographic attributes in this study were derived from publicly available digital elevation data and software tools, as detailed in Table 1.

Received: 8 April 2025; Accepted: 5 September 2025

Published online: 08 October 2025

## References

- Duncanson, L. et al. The Importance of Consistent Global Forest Aboveground Biomass Product Validation. *Surv. Geophys.* **40**(4), 979–999. <https://doi.org/10.1007/s10712-019-09538-8> (2019).
- Mitchard, E. T. et al. Uncertainty in the spatial distribution of tropical forest biomass: A comparison of pan-tropical maps. *Carbon Bal. Manage.* **8**(1), 10. <https://doi.org/10.1186/1750-0680-8-10> (2013).
- Rozendaal, D. M. A. et al. Aboveground forest biomass varies across continents, ecological zones and successional stages: refined IPCC default values for tropical and subtropical forests. *Environ. Res. Lett.* **17**(1), 014047. <https://doi.org/10.1088/1748-9326/ac45b3> (2022).
- Khanal, S. et al. Disentangling contributions of allometry, species composition and structure to high aboveground biomass density of high-elevation forests. *For. Ecol. Manag.* **554**, 121679. <https://doi.org/10.1016/j.foreco.2023.121679> (2024).
- Rawat, G. S., Lama, D. The Himalayan vegetation along horizontal and vertical gradients. In: Prins HHT, Namgail T (eds) Bird Migration across the Himalayas: Wetland Functioning amidst Mountains and Glaciers. Cambridge University Press, p 189–204, <https://doi.org/10.1017/9781316335420.015> (2017).
- Thapa, U. et al. Tree growth across the Nepal Himalaya during the last four centuries. *Prog. Phys. Geogr. Earth Environ.* **41**(4), 478–495. <https://doi.org/10.1177/0309133317714247> (2017).
- Gaire, N. P. et al. Drought (scPDSI) reconstruction of trans-Himalayan region of central Himalaya using Pinus wallichiana tree-rings. *Palaeogeogr. Palaeoclimatol. Palaeoecol.* **514**, 251–264. <https://doi.org/10.1016/j.palaeo.2018.10.026> (2019).
- Cook, E. R., Krusic, P. J. & Jones, P. D. Dendroclimatic signals in long tree-ring chronologies from the Himalayas of Nepal. *Int. J. Climatol.* **23**(7), 707–732. <https://doi.org/10.1002/joc.911> (2003).
- Bohner, J. General climatic controls and topoclimatic variations in Central and High Asia. *Boreas* **35**(2), 279–295. <https://doi.org/10.1111/j.1502-3885.2006.tb01158.x> (2006).
- Ehbrecht, M. et al. Global patterns and climatic controls of forest structural complexity. *Nat. Commun.* **12**(1), 1–12. <https://doi.org/10.1038/s41467-020-20767-z> (2021).
- Gnann, S. et al. The influence of topography on the global terrestrial water cycle. *Rev. Geophys.* **63**(1), e2023RG000810. <https://doi.org/10.1029/2023RG000810> (2025).
- Meetei, P. N. et al. Spatio-temporal analysis of snow cover and effect of terrain attributes in the Upper Ganga River Basin, Central Himalaya. *Geocarto Int.* 1–21. <https://doi.org/10.1080/10106049.2020.1762764> (2020).
- McNichol, B. H. et al. Topography-driven microclimate gradients shape forest structure, diversity, and composition in a temperate refugial forest. *Plant-Environ. Interact.* **5**(3), e10153. <https://doi.org/10.1002/pei3.10153> (2024).
- Anders, A. et al. Spatial patterns of precipitation and topography in the Himalaya. *Spec. Paper Geol. Soc. Am.* **398**, 39–53. [https://doi.org/10.1130/2006.2398\(03\)](https://doi.org/10.1130/2006.2398(03)) (2006) (copyright: Copyright 2019 Elsevier B.V., All rights reserved).
- Xian, Y. et al. Can topographic effects on solar radiation be ignored: Evidence from the Tibetan plateau. *Geophys. Res. Lett.* **51**(6), e2024GL108653. <https://doi.org/10.1029/2024GL108653> (2024).
- Streher, A. S. et al. Land surface phenology in the tropics: The role of climate and topography in a snow-free mountain. *Ecosystems* **20**(8), 1436–1453. <https://doi.org/10.1007/s10021-017-0123-2> (2017).
- Bunn, A. G. et al. Spatiotemporal variability in the climate growth response of high elevation Bristlecone Pine in the White Mountains of California. *Geophys. Res. Lett.* **45**(24), 13,312–13,321. <https://doi.org/10.1029/2018GL080981> (2018).
- Hoyleman, Z. H. et al. Hillslope topography mediates spatial patterns of ecosystem sensitivity to climate. *J. Geophys. Res. Biogeosci.* **123**(2), 353–371. <https://doi.org/10.1002/2017JG004108> (2018).
- Raich, J. W. et al. Temperature influences carbon accumulation in Moist Tropical Forests. *Ecology* **87**(1), 76–87. <https://doi.org/10.1890/0050-0023> (2006).
- Jenkins, J. C., Birdsey, R. A. & Pan, Y. Biomass and NPP Estimation for the Mid-Atlantic Region (USA) using Plot-level Forest Inventory Data. *Ecol. Appl.* **11**(4), 1174–1193 (2001).
- Holm, J. A. et al. Shifts in biomass and productivity for a subtropical dry forest in response to simulated elevated hurricane disturbances. *Environ. Res. Lett.* **12**(2), 025007. <https://doi.org/10.1088/1748-9326/aa583c> (2017).
- Johnson, M. O. et al. Variation in stem mortality rates determines patterns of above-ground biomass in Amazonian forests: Implications for dynamic global vegetation models. *Glob. Change Biol.* **22**(12), 3996–4013. <https://doi.org/10.1111/gcb.13315> (2016).

23. Clark, D. A. et al. Measuring Net Primary Production in Forests: Concepts and Field Methods. *Ecol. Appl.* **11**(2), 356–370 (2001).
24. Whittaker, R. H. et al. The Hubbard Brook ecosystem study: Forest biomass and production. *Ecol. Monogr.* **44**(2), 233–254. <https://doi.org/10.2307/1942313> (1974).
25. Moser, G. et al. Elevation effects on the carbon budget of tropical mountain forests (S Ecuador): The role of the belowground compartment. *Glob. Change Biol.* **17**(6), 2211–2226. <https://doi.org/10.1111/j.1365-2486.2010.02367.x> (2011).
26. Rai, I.D., Padalia, H., Singh, G., et al. Vegetation dry matter dynamics along treeline ecotone in Western Himalaya, India. *Trop. Ecol.* **1**–12. <https://doi.org/10.1007/s42965-020-00067-9> (2020).
27. Garkoti, S. & Singh, S. Variation in net primary productivity and biomass of forests in the high mountains of Central Himalaya. *J. Veg. Sci.* **6**(1), 23–28. <https://doi.org/10.2307/3236252> (1995).
28. Rosenzweig, M. L. Net primary productivity of terrestrial communities: Prediction from climatological data. *Am. Nat.* **102**(923), 67–74. <https://doi.org/10.1086/282523> (1968) [arXiv:2459049](https://arxiv.org/abs/2459049).
29. Yang, Y., Long, D. & Shang, S. Remote estimation of terrestrial evapotranspiration without using meteorological data. *Geophys. Res. Lett.* **40**(12), 3026–3030. <https://doi.org/10.1002/grl.50450> (2013).
30. Stephenson, N. Actual evapotranspiration and deficit: Biologically meaningful correlates of vegetation distribution across spatial scales. *J. Biogeogr.* **25**(5), 855–870. <https://doi.org/10.1046/j.1365-2699.1998.00233.x> (1998).
31. Khanal, S. et al. Environmental correlates of the forest carbon distribution in the Central Himalayas. *Ecol. Evol.* **14**(6), e11517. <https://doi.org/10.1002/ece3.11517> (2024).
32. Korup, O. et al. Giant landslides, topography, and erosion. *Earth Planet. Sci. Lett.* **261**(3), 578–589. <https://doi.org/10.1016/j.epsl.2007.07.025> (2007).
33. Alvioli, M. et al. Topography-driven satellite imagery analysis for landslide mapping. *Geomat. Nat. Haz. Risk* **9**(1), 544–567. <https://doi.org/10.1080/19475705.2018.1458050> (2018).
34. Restrepo, C., Vitousek, P. & Neville, P. Landslides significantly alter land cover and the distribution of biomass: An example from the Ninole ridges of Hawaii. *Plant Ecol.* **166**(1), 131–143. <https://doi.org/10.1023/A:1023225419111> (2003).
35. Gerlitz, L., Conrad, O. & Böhner, J. Large-scale atmospheric forcing and topographic modification of precipitation rates over High Asia – a neural-network-based approach. *Earth Syst. Dyn.* **6**(1), 61–81. <https://doi.org/10.5194/esd-6-61-2015> (2015).
36. Zhang, X. et al. Evaluation of Reanalysis Surface Incident Solar Radiation Data in China. *Sci. Rep.* **10**(1), 3494. <https://doi.org/10.1038/s41598-020-60460-1> (2020).
37. Song, C. et al. Homogenization of surface temperature data in High Mountain Asia through comparison of reanalysis data and station observations. *Int. J. Climatol.* **36**(3), 1088–1101. <https://doi.org/10.1002/joc.4403> (2016).
38. Aguilar, C., Herrero, J. & Polo, M. J. Topographic effects on solar radiation distribution in mountainous watersheds and their influence on reference evapotranspiration estimates at watershed scale. *Hydrol. Earth Syst. Sci.* **14**(12), 2479–2494. <https://doi.org/10.5194/hess-14-2479-2010> (2010).
39. Williams, C. J., McNamara, J. P. & Chandler, D. G. Controls on the temporal and spatial variability of soil moisture in a mountainous landscape: The signature of snow and complex terrain. *Hydrol. Earth Syst. Sci.* **13**(7), 1325–1336. <https://doi.org/10.5194/hess-13-1325-2009> (2009).
40. Boer, M., Barrio, G. & Puigdefabregas, J. Mapping soil depth classes in dry Mediterranean areas using terrain attributes derived from a digital elevation model. *Geoderma* **72**(1), 99–118. [https://doi.org/10.1016/0016-7061\(96\)00024-9](https://doi.org/10.1016/0016-7061(96)00024-9) (1996).
41. Khanal, S. & Boer, M. M. Plot-level estimates of aboveground biomass and soil organic carbon stocks from Nepal's forest inventory. *Sci. Data* **10**(1), 406. <https://doi.org/10.1038/s41597-023-02314-9> (2023).
42. Stephenson, N. L. Climatic control of vegetation distribution: The role of the water balance. *Am. Nat.* **135**(5), 649–670. [www.jstor.org/stable/2462028](https://www.jstor.org/stable/2462028) (1990).
43. DFRS. *State of Nepal's forests* (Kathmandu, Nepal, Department of Forest Research and Survey (DFRS), 2015).
44. Spacesystems, N. Team UAS ASTER global digital elevation model V003 [Data set]. <https://doi.org/10.5067/ASTER/ASTGTM.003> (2019).
45. Wilson, J. Calculating land surface parameters. In *Environmental Applications of Digital Terrain Modeling*. John Wiley & Sons, Ltd, p 53–149. <https://doi.org/10.1002/9781118938188.ch3> (2018).
46. Olaya, V. Chapter 6 basic land-surface parameters. In: Hengl T, Reuter HI (eds) *Geomorphometry, Developments in Soil Science*, vol 33. Elsevier, p 141–169. [https://doi.org/10.1016/S0166-2481\(08\)00006-8](https://doi.org/10.1016/S0166-2481(08)00006-8) (2009).
47. Wilson, J. P. & Gallant, J. C. *Terrain Analysis: Principles and Applications* (John Wiley & Sons, 2000).
48. Bohner, J. & Antonic, O. Chapter 8 land-surface parameters specific to topo-climatology. In Hengl T, Reuter HI (eds) *Developments in Soil Science*, vol 33. Elsevier, p 195–226. [https://doi.org/10.1016/S0166-2481\(08\)00008-1](https://doi.org/10.1016/S0166-2481(08)00008-1) (2009).
49. Conrad, O. et al. System for automated geoscientific analyses (SAGA) v. 21. 4. *Geosci. Model Dev.* **8**(7), 1991–2007. <https://doi.org/10.5194/gmd-8-1991-2015> (2015) <https://www.geosci-model-dev.net/8/1991/2015/>.
50. Renard, K. et al. *Predicting soil erosion by water: A guide to conservation planning with the Revised Universal Soil Loss Equation (RUSLE)* Vol. 703 (Department of Agriculture, Agriculture handbook, U.S., 1996).
51. Guisan, A., Weiss, S. B. & Weiss, A. D. GLM versus CCA spatial modeling of plant species distribution. *Plant Ecol.* **143**(1), 107–122. <https://doi.org/10.1023/A:1009841519580> (1999).
52. Ludwig, J. A. et al. Vegetation patches and runoff-erosion as interacting ecohydrological processes in semiarid landscapes. *Ecology* **86**(2), 288–297. <https://doi.org/10.1890/03-0569> (2005).
53. Beven, K. J. & Kirkby, M. J. A physically based, variable contributing area model of basin hydrology / Un modele a base physique de zone d'appel variable de l'hydrologie du bassin versant. *Hydrol. Sci. Bull.* **24**(1), 43–69. <https://doi.org/10.1080/02626667909491834> (1979).
54. Kopecký, M., Macek, M. & Wild, J. Topographic wetness index calculation guidelines based on measured soil moisture and plant species composition. *Sci. Total Environ.* **757**, 143785. <https://doi.org/10.1016/j.scitotenv.2020.143785> (2021).
55. Karger, D. N. et al. Climatologies at high resolution for the earth's land surface areas. *Sci. Data* **4**, 170122. <https://doi.org/10.1038/sdata.2017.122> (2017).
56. Kumar, S.V., & Yoon, Y. High Mountain Asia LIS model terrestrial hydrological parameters, version 1. [SNOW WATER EQUIVALENT]. misc, NASA national snow and ice data center distributed active archive center., <https://doi.org/10.5067/ENXLS5FDN5V8C> (2019).
57. Samani, Z. Estimating solar radiation and evapotranspiration using minimum climatological data. *J. Irrig. Drain. Eng.* **126**(4), 265–267. [https://doi.org/10.1061/\(ASCE\)0733-9437\(2000\)126:4\(265\)](https://doi.org/10.1061/(ASCE)0733-9437(2000)126:4(265)) (2000).
58. Ravazzani, G. et al. Modified Hargreaves-Samani equation for the assessment of reference evapotranspiration in Alpine river basins. *J. Irrig. Drain. Eng.* **138**(7), 592–599. [https://doi.org/10.1061/\(ASCE\)IR.1943-4774.0000453](https://doi.org/10.1061/(ASCE)IR.1943-4774.0000453) (2012).
59. Wood, S. N. Generalized Additive Models: An Introduction with R. *CRC Press* <https://doi.org/10.1201/9781315370279> (2017).
60. Fasiolo, M., Goude, Y., Nedellec, R., et al. Fast calibrated additive quantile regression. misc, [arxiv:1707.03307](https://arxiv.org/abs/1707.03307) (2017).
61. Kerby, D.S. The simple difference formula: An approach to teaching nonparametric correlation. *Comprehensive Psychology* **3**:11. <https://doi.org/10.2466/11.IT.3.1> (2014).
62. Körner, C. Alpine plant life: Functional plant ecology of high mountain ecosystems. *Springer Sci. Bus. Media* <https://doi.org/10.1007/978-3-642-18970-8> (2003).
63. Muscarella, R. et al. Effects of topography on tropical forest structure depend on climate context. *J. Ecol.* **108**(1), 145–159. <https://doi.org/10.1111/1365-2745.13261> (2020).



64. Jucker, T. et al. Topography shapes the structure, composition and function of tropical forest landscapes. *Ecol. Lett.* **21**(7), 989–1000. <https://doi.org/10.1111/ele.12964> (2018).
65. Holtmeier, F. K. et al. Mountain birch, tree line and climate change. *Ger. Res.* **30**(3), 25–28. <https://doi.org/10.1002/germ.200990005> (2008).
66. Wambulwa, M. C. et al. Spatiotemporal maintenance of flora in the Himalaya biodiversity hotspot: Current knowledge and future perspectives. *Ecol. Evol.* **11**(16), 10794–10812. <https://doi.org/10.1002/ece3.7906> (2021).
67. Peckham, S. D. Profile, plan and streamline curvature: A simple derivation and applications. *Proc. Geomorphometry* **4**, 27–30 (2011).
68. Burt, T. P. & Butcher, D. P. Topographic controls of soil moisture distributions. *J. Soil Sci.* **36**(3), 469–486. <https://doi.org/10.1111/j.1365-2389.1985.tb00351.x> (1985).
69. Talebi, A., Uijlenhoet, R. & Troch, P. A. Soil moisture storage and hillslope stability. *Nat. Hazards Earth Syst. Sci.* **7**(5), 523–534. <https://doi.org/10.5194/nhess-7-523-2007> (2007).
70. Ohlmacher, G. C. Plan curvature and landslide probability in regions dominated by earth flows and earth slides. *Eng. Geol.* **91**(2), 117–134. <https://doi.org/10.1016/j.enggeo.2007.01.005> (2007).
71. Sørensen, R., Zinko, U. & Seibert, J. On the calculation of the topographic wetness index: Evaluation of different methods based on field observations. *Hydrol. Earth Syst. Sci.* **10**(1), 101–112. <https://doi.org/10.5194/hess-10-101-2006> (2006).
72. Schmidt, S., Tresch, S. & Meusburger, K. Modification of the RUSLE slope length and steepness factor (LS-factor) based on rainfall experiments at steep alpine grasslands. *MethodsX* **6**, 219–229. <https://doi.org/10.1016/j.mex.2019.01.004> (2019).
73. Dyer, J. M. Assessing topographic patterns in moisture use and stress using a water balance approach. *Landsc. Ecol.* **24**(3), 391–403. <https://doi.org/10.1007/s10980-008-9316-6> (2009).
74. Yang, Y. et al. Sensitivity of potential evapotranspiration to meteorological factors and their elevational gradients in the Qilian Mountains, northwestern China. *J. Hydrol.* **568**, 147–159. <https://doi.org/10.1016/j.jhydrol.2018.10.069> (2019).
75. Lambert, L. & Chitrakar, B. D. Variation of potential evapotranspiration with elevation in Nepal. *Mt. Res. Dev.* **9**(2), 145–152. <https://doi.org/10.2307/3673477> (1989).
76. Dai, W. et al. Spatiotemporal variation of potential evapotranspiration and meteorological drought based on multi-source data in Nepal. *Nat. Hazards Res.* **3**(2), 271–279. <https://doi.org/10.1016/j.nhres.2023.04.007> (2023).
77. Henning, I. & Henning, D. Potential evapotranspiration in mountain geoecosystems of different altitudes and latitudes. *Mt. Res. Dev.* **1**(3/4), 267–274. <https://doi.org/10.2307/3673064> (1981).
78. Neto, A. A. M. et al. Interactions between snow cover and evaporation lead to higher sensitivity of streamflow to temperature. *Commun. Earth Environ.* **1**(1), 1–7. <https://doi.org/10.1038/s43247-020-00056-9> (2020).
79. Li, X. et al. The mechanical origin of snow avalanche dynamics and flow regime transitions. *The Cryosphere* **14**(10), 3381–3398. <https://doi.org/10.5194/tc-14-3381-2020> (2020).
80. Kulakowski, D., Rixen, C. & Bebi, P. Changes in forest structure and in the relative importance of climatic stress as a result of suppression of avalanche disturbances. *For. Ecol. Manag.* **223**(1), 66–74. <https://doi.org/10.1016/j.foreco.2005.10.058> (2006).
81. Metz, J. J. Vegetation dynamics of several little disturbed temperate forests in east Central Nepal. *Mount. Res. Dev.* **17**(4), 333–351 (1997).
82. Chidi, C. L. Human settlements in high altitude region Nepal. *Geogr. J. Nepal* **7**, 1–6. <https://doi.org/10.3126/gjn.v7i0.17436>. <https://nepjol.info/index.php/gjn/article/view/17436> (2009).
83. Ichayanagi, K. et al. Precipitation in nepal between 1987 and 1996. *Int. J. Climatol.* **27**(13), 1753–1762. <https://doi.org/10.1002/joc.1492> (2007).
84. Talchabhadel, R. et al. Spatio-temporal variability of extreme precipitation in Nepal. *Int. J. Climatol.* **38**(11), 4296–4313. <https://doi.org/10.1002/joc.5669> (2018).
85. McAdoo, B. G. et al. Roads and landslides in Nepal: How development affects environmental risk. *Nat. Hazards Earth Syst. Sci.* **18**(12), 3203–3210. <https://doi.org/10.5194/nhess-18-3203-2018> (2018).
86. Adeniyi, O. D. & Maerker, M. Explorative analysis of varying spatial resolutions on a soil type classification model and its transferability in an agricultural lowland area of Lombardy, Italy. *Geoderma Region.* **37**, e00785. <https://doi.org/10.1016/j.geodrs.2024.e00785> (2024).
87. Horst-Heinen, T. Z. et al. Soil depth prediction by digital soil mapping and its impact in pine forestry productivity in south brazil. *For. Ecol. Manag.* **488**, 118983. <https://doi.org/10.1016/j.foreco.2021.118983> (2021).
88. Guevara Mario, A. N. D. & Vargas, R. Downscaling satellite soil moisture using geomorphometry and machine learning. *PLoS ONE* **14**(9), 1–20. <https://doi.org/10.1371/journal.pone.0219639> (2019).
89. McIntire, E. J. B., Piper, F. I. & Fajardo, A. Wind exposure and light exposure, more than elevation-related temperature, limit tree line seedling abundance on three continents. *J. Ecol.* **104**(5), 1379–1390. <https://doi.org/10.1111/1365-2745.12599> (2016).
90. Mitchell, S. Wind as a natural disturbance agent in forests: a synthesis. *For. Int. J. Forest Res.* **86**(2), 147–157. <https://doi.org/10.1093/forestry/cps058> (2012).

## Acknowledgements

We are grateful for the financial support provided by the Australian Government Research Training Program (RTP) scholarship.

## Author contributions

S.K. led the conceptualization, data acquisition, and analysis of the study, including writing an original draft manuscript. M.M.B., R.H.N. and B.E.M. advised on the data processing, modelling and interpretation of the results. The first draft of the manuscript was written by SK and all authors commented on previous versions of the manuscript. All authors read and approved the final manuscript.

## Declarations

## Competing interests

The authors declare no competing interests.

## Additional information

**Supplementary Information** The online version contains supplementary material available at <https://doi.org/10.1038/s41598-025-19127-y>.

**Correspondence** and requests for materials should be addressed to S.K.

**Reprints and permissions information** is available at [www.nature.com/reprints](http://www.nature.com/reprints).

**Publisher's note** Springer Nature remains neutral with regard to jurisdictional claims in published maps and institutional affiliations.

**Open Access** This article is licensed under a Creative Commons Attribution-NonCommercial-NoDerivatives 4.0 International License, which permits any non-commercial use, sharing, distribution and reproduction in any medium or format, as long as you give appropriate credit to the original author(s) and the source, provide a link to the Creative Commons licence, and indicate if you modified the licensed material. You do not have permission under this licence to share adapted material derived from this article or parts of it. The images or other third party material in this article are included in the article's Creative Commons licence, unless indicated otherwise in a credit line to the material. If material is not included in the article's Creative Commons licence and your intended use is not permitted by statutory regulation or exceeds the permitted use, you will need to obtain permission directly from the copyright holder. To view a copy of this licence, visit <http://creativecommons.org/licenses/by-nc-nd/4.0/>.

© The Author(s) 2025